Giant photocurrent enhancement by transition metal doping in quantum dot sensitized solar cells

Gaurab Rimal, Artem K. Pimachev, Andrew J. Yost, Uma Poudyal, Scott Maloney, Wenyong Wang, TeYu Chien, Yuri Dahnovsky, and Jinke Tang

Citation: Appl. Phys. Lett. **109**, 103901 (2016); doi: 10.1063/1.4962331
View online: http://dx.doi.org/10.1063/1.4962331
View Table of Contents: http://aip.scitation.org/toc/apl/109/10
Published by the American Institute of Physics

Giant photocurrent enhancement by transition metal doping in quantum dot sensitized solar cells

Gaurab Rimal, Artem K. Pimachev, Andrew J. Yost, Uma Poudyal, Scott Maloney, Wenyong Wang, TeYu Chien, Yuri Dahnovsky,[a] and Jinke Tang[a]
Department of Physics and Astronomy, University of Wyoming, Laramie, Wyoming 82071, USA

(Received 16 May 2016; accepted 24 August 2016; published online 6 September 2016)

A huge enhancement in the incident photon-to-current efficiency of PbS quantum dot (QD) sensitized solar cells by manganese doping is observed. In the presence of Mn dopants with relatively small concentration (4 at. %), the photoelectric current increases by an average of 300% (up to 700%). This effect cannot be explained by the light absorption mechanism because both the experimental and theoretical absorption spectra demonstrate several times decreases in the absorption coefficient. To explain such dramatic increase in the photocurrent we propose the electron tunneling mechanism from the LUMO of the QD excited state to the Zn_2SnO_4 (ZTO) semiconductor photoanode. This change is due to the presence of the Mn instead of Pb atom at the QD/ZTO interface. The *ab initio* calculations confirm this mechanism. This work proposes an alternative route for a significant improvement of the efficiency for quantum dot sensitized solar cells. *Published by AIP Publishing*. [http://dx.doi.org/10.1063/1.4962331]

The quest for high efficiency solar cells has led to the search of new materials for sensitizers and photoconductor (oxide) electrodes. The efficiency of quantum dot sensitized solar cells (QDSSCs) has increased slowly since quantum dots (QDs) were first used as sensitizers in the solar cells. Even though the power conversion efficiency has reached about 12%,[1] the overall efficiency is relatively low compared to silicon based photovoltaics as well as the newer perovskite based solar cells.[2] Factors such as carrier trapping and recombination, low charge transfer and band misalignment are the major reasons for low efficiency in QDSSC. Many of these issues have been studied to boost the overall efficiency but the results are still not encouraging. One possibility to improve the efficiency is to employ transition metal (TM) as dopants in the QD sensitizers. The TM dopants in QDs have the potential to introduce impurity states in the band gap and enhance absorption.[3–5]

PbS QDs have been extensively studied as a sensitizer because of their ability to be efficient in the multiexciton generation[6] and strong confinement effect.[7] PbS QDs also show some of the better power conversion efficiencies (PCE) of various other materials, with an efficiency of 10.7% in recent literature.[8] However, effort in the investigation of Mn doped PbS QDs is needed in order to understand whether the Mn impurities introduce new states within the band gap or change the band structure itself. Recent works on Mn:PbS have indicated the broadening of the band gap rather than the addition of the impurity energy levels inside the band gap.[9] In the case of ZnS, the Mn *d*-states lie within the band gap, and these mid-band-gap states contribute to the absorption as well as electron transfer due to the long lifetimes of the spin forbidden transitions.[5] This situation is also true in CdS and CdSe,[4] although for large QDs, the Mn *d*-states may be located near or above the conduction band.[10,11] In the latter case, strong *sp-d* hybridization between the Mn *d*-states and semiconductor conduction band may induce exchange splitting of the conduction band and narrow the band gap, which alters the photoconversion efficiency in different ways.[3] In PbS, however, due to its small band gap the effect of the *sp–d* hybridization seems to broaden the band gap and the absorption decreases with the Mn doping.[9] At the first glance, this system seems to have less potential for a high efficiency solar cell; however, we have found a giant enhancement in the QDSSC performance using Mn doped PbS QDs.

In this study, PbS and Mn:PbS QDs are prepared with pulsed laser deposition (PLD) technique.[12,13] The presence of Mn in PbS is confirmed with electron paramagnetic resonance (EPR) spectroscopy. The band gap of the QDs was found to increase with the addition of manganese in both computational and scanning tunneling microscopy/spectroscopy (STM/S) investigations. This bandgap increase is believed to be associated with the decrease of the light absorption upon addition of Mn dopants. Surprisingly, the photovoltaic measurements of doped and undoped QDs attached to Zn_2SnO_4 (ZTO) nanowire photoelectrode show that the devices with Mn doped PbS QDs have much higher incident photon-to-current efficiency (IPCE), which is attributed to more efficient electron tunneling to the ZTO nanowire from the QD excited states. This conclusion is confirmed by *ab-initio* calculations on the electron transfer from the Mn doped PbS QD to the ZTO electrode, which show reduced tunneling barrier heights for the transferring electrons.

The dopant and structural properties of the QDs are characterized by x-ray diffraction (XRD), EPR, and STM/S. Figure 1(a) shows the XRD pattern of a doped sample along with a PbS reference, which verifies the PbS rock salt crystal structure. There are also minor impurity peaks due to Pb metal. The metallic Pb precipitation is inherent to the preparation process but does not change the semiconducting nature of the films for both doped and undoped PbS samples. The energy dispersive x-ray spectroscopy (EDX) shows that

[a]Electronic addresses: yurid@uwyo.edu and jtang2@uwyo.edu

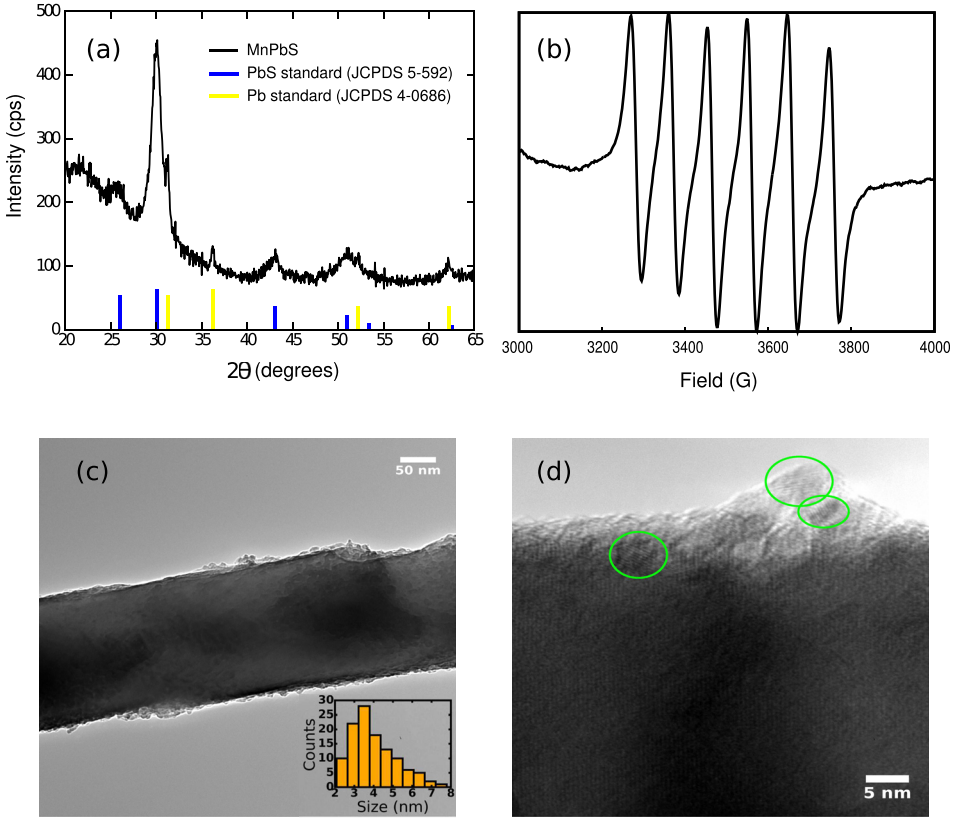

FIG. 1. (a) X-ray diffraction pattern of Mn doped PbS. Also shown are the PbS and Pb standards. (b) Electron paramagnetic resonance spectrum of Mn doped PbS at room temperature. (c) Transmission electron micrograph of a nanowire containing Mn doped PbS QDs. Inset: histogram showing particle size distribution. (d) Zoomed region of the nanowire showing QDs on its surface.

the average Mn concentration is about 4 at. %. The Mn concentration is found to remain less than 5 at. % even when we start out from a higher nominal concentration in the PLD target, which points to a solubility limit of substitutional Mn within the PbS lattice.

Electron paramagnetic resonance (EPR) (Figure 1(b)) is also used to check for the Mn incorporation into the QDs. The Mn presence is confirmed by the resonance lines with the well-resolved hyperfine splitting of the central Mn^{2+} sextet in the EPR spectra. The hyperfine constant obtained from the EPR spectrum, is 266 ± 1 MHz, which is in agreement with the previously obtained values.[14–16] The g factor is close to 2. Moreover, we also observe the forbidden $M = \pm 1$ transitions, which are seen as the shoulder peaks. These forbidden transitions have been explained as the third order perturbation due to the spin contribution to the total Hamiltonian resulting from the admixture of fine and hyperfine structure terms.[17] In comparison with the previous calculations, the hyperfine splitting values indicate that there are more Mn ions residing on the surface than inside the QDs. Such a Mn position on the QD surface could strongly influence the tunneling current to the ZTO electrode in the experiments as we discuss later in more detail.

Figure 1(c) shows a transmission electron micrograph (TEM) of a nanowire containing Mn doped PbS QDs, which are deposited on the nanowire via PLD. The particle size distribution is shown in the inset. A high resolution TEM image of a magnified region of the nanowire showing QDs on its surface is provided in Fig. 1(d).

The optical absorption spectra in the near infrared (NIR) region (Figure 2(a)) are taken for the samples identically deposited on quartz. It demonstrates that the undoped QDs absorb more than the Mn doped QDs. Similar dependence is also confirmed from the *ab initio* calculations for the small quantum dots ($Pb_{28}S_{28}$ for undoped and $Pb_{26}Mn_2S_{28}$ for doped QDs), as shown in Fig. 2(b). The *sp-d* hybridization due to the sulfur *sp* electron and Mn *d* electrons results in the blue shift of the band gap, which is counted from the first exciton peak as depicted in Fig. 2(b). It is clearly demonstrated that the absorption for undoped QD is much higher than that for Mn doped QDs. The computational absorption wavelength region lies on the blue side compared to the experimental observation, but the discussion is valid for QDs of all sizes. Exciton peak in experimental absorption spectrum (see Figure 2(a)) is not seen because of large QD size distribution. The additional confirmation of band gap broadening is obtained from scanning tunneling spectroscopy (STS) measurements from the dI/dV spectra obtained for quantum dots of similar size (Figure 3).

The most striking result of this study appears in the IPCE spectra. The measurements were made on devices with the QDs deposited directly on the ZTO nanowire photoelectrodes. Figure 4 shows the comparison of the IPCE spectra between doped and undoped PbS QDs for two sets of samples. For the samples shown, the photoelectric current is increased between 100% and 700% upon the Mn doping. The average increase among all experiments on various samples is 300% measured at wavelength $\lambda = 800$ nm. One would expect, however, a decrease of the IPCE value because the absorption is about 2.5 times less due to the doping. In reality, we observe the huge increase in the photocurrent. The photoelectric current is mainly due to three factors: (a) light absorption, (b) exciton lifetime, and (c) electron tunneling through the semiconductor/quantum dot interface. The experimental and computational absorption spectra (Figure 2) lead us to believe that the mechanism of such a

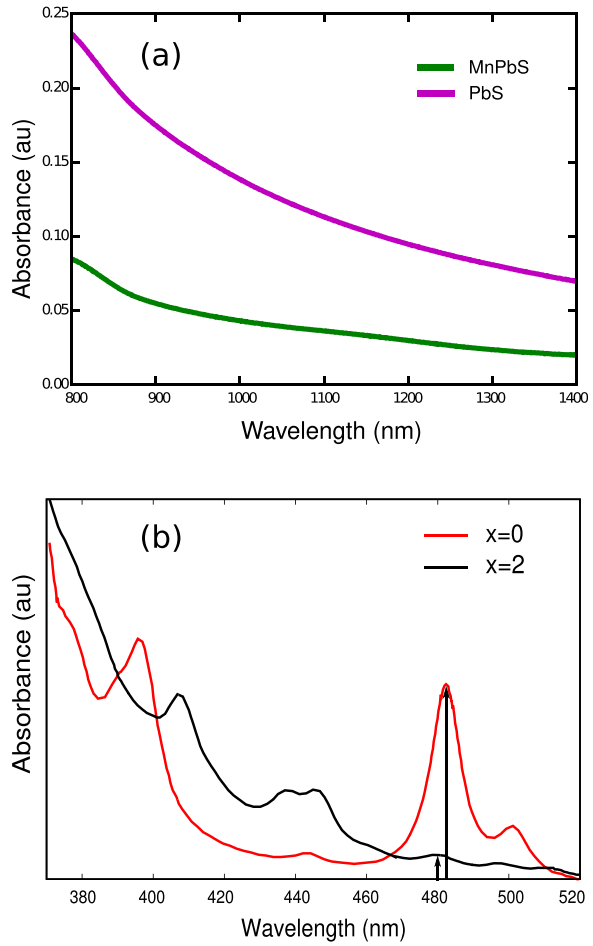

FIG. 2. (a) Comparison of the absorption spectra of PbS and Mn:PbS. (b) Calculated absorption spectra for $Pb_{28-x}Mn_xS_{28}$ with $x = 0$ and $x = 2$. The arrows point to the exciton peaks to show the relative absorption for doped and undoped QDs.

giant enhancement in the photocurrent does not lie in light absorption. The exciton lifetime in Mn doped PbS is three times smaller than undoped QDs due to the presence of Mn-induced carrier traps.[18] The only mechanism that could explain the IPCE increase is the electron tunneling effect. We thoroughly study this mechanism computationally as described below.

The main hypothesis is that the tunneling strongly depends on the nature of a QD metal atom (Mn or Pb) that is the closest to the semiconductor (ZTO) surface, at which the

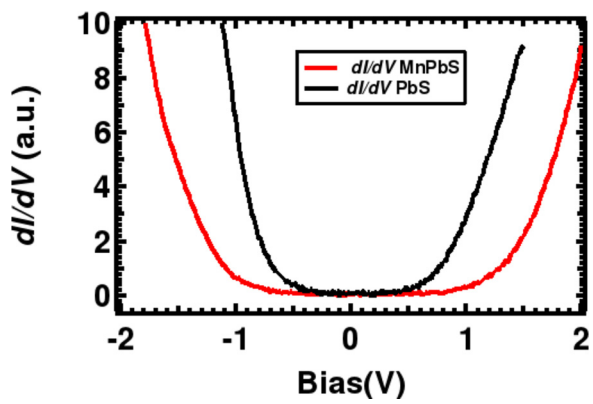

FIG. 3. *dI*/*dV* spectra for the undoped (the black curve) and Mn doped (the red curve) quantum dots of similar size.

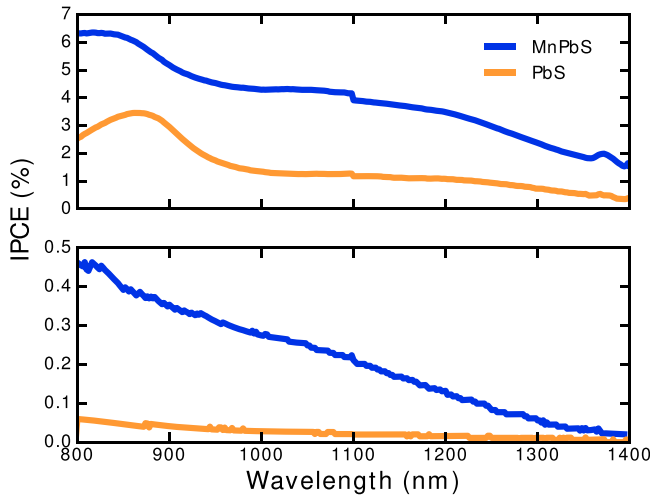

FIG. 4. Comparison of incident photon to electron conversion efficiency (IPCE) spectra of two groups of samples.

excited electron transfers through (see Figure 5). Electron tunneling can be considered as a nonadiabatic electron transfer where the rate constant can be described in terms of the time-dependent perturbation theory with the electron transfer rate where V is the electron transition matrix element and is the electron density of states on the ZTO surface. In this model, we assume that the electron transfer takes place from the QD LUMO orbital (the bottom of the QD conduction band). If the exciton is excited to the higher conduction electronic states, fast relaxation due to electron-phonon interaction brings the electron down to the LUMO.[19] The transfer electric current to the ZTO semiconductor can be described in terms of the Bardeen's Hamiltonian and therefore the expression for the current from the LUMO is expressed in

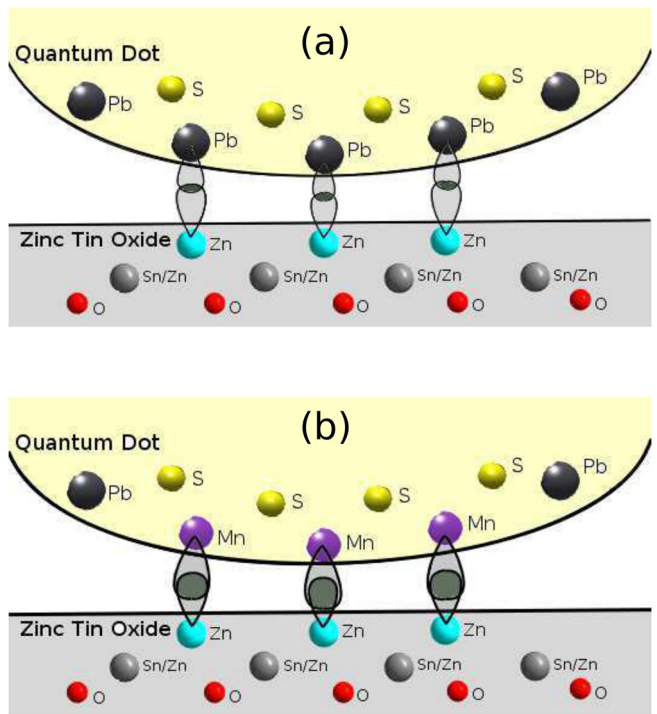

FIG. 5. Schematic representation of the interface between PbS quantum dot and ZTO surface for pure PbS (a) and Mn doped PbS (b). The overlap of the orbitals is presented by shaded regions, which is enhanced when Pb is replaced with Mn.

terms of nonequilibrium Green's functions, which are again proportional to $|V|^2$.[20] Thus, we have to calculate the current for $|V_{Mn/ZTO}|^2$ and $|V_{Pb/ZTO}|^2$. In the simplest estimations of the current ratio, we assume that the density of states at the ZTO surface remains unchanged in both cases. Thus, $J_{Mn/ZTO}/J_{PbZTO} = |V_{Mn/ZTO}|^2/|V_{Pb/ZTO}|^2$. This ratio provides a good estimation for the photocurrents rather than the exact numerical calculation.

The electron transition matrix elements have been obtained from the quantum chemical calculations where the electron is initially located at the LUMO on the QD side. The final electron state is located on the ZTO side. We have checked two cases where one or three metal atoms (Mn or Pb) touch the ZTO interface promoting the electron tunneling. The results of the computations are presented in Table I. The $|V_{Mn/ZTO}|^2/|V_{Pb/ZTO}|^2$ ratio is approximately equal to 6.9. The estimated current ratio is of the same order of magnitude as experimentally observed in Figure 4. These calculations confirm that the mechanism of the photocurrent enhancement originates from the electron tunneling. The EPR spectra (see Figure 1(b)) indicate that more Mn dopants are located on the QD surface than the interior and therefore the assumption that the electron tunnels through the Mn atom is plausible and confirms the tunneling mechanism described above. Figure 5 demonstrates the spatial overlap of the wavefunctions. Due to greater wavefunction overlap, which reduces the barrier height for the electron tunneling, more electrons are collected by the nanowire photoanode leading to higher photocurrents in the Mn doped samples.

Despite the decrease of the QD absorption in the presence of small amount of Mn dopants, we have found the giant enhancement in the photocurrent by up to 700%. We have proposed a mechanism of the photocurrent increase that is based on the change of the electron-tunneling rate in the presence of the Mn atom located at the QD/ZTO interface. The *ab initio* quantum chemical calculations confirm this mechanism. The results obtained in this work point to an alternative route for significant improvement of the QDSSC efficiency.

Manganese doped lead sulfide nanoparticles were deposited directly on Zn_2SnO_4 (ZTO) nanowires, quartz, and Si via pulsed laser deposition (PLD).[12] The nanowire synthesis and device preparation are described elsewhere.[21] A Nd:YAG laser operating at a wavelength of 266 nm and a pulse energy of 280 mJ was used to ablate a pre-prepared Mn:PbS target. The deposition was carried out at pressures of 4–6 μTorr. No heat was applied to the substrate during deposition.

After the deposition, the sensitized nanowire film was SILAR coated with CdS to prevent rapid degradation of the nanoparticles in polysulfide electrolyte and to eliminate the effect on the regeneration due to the presence of Mn.[22] We confined our optical characterization in the NIR window to minimize any contribution from the CdS layer. A standard Cu_2S counter electrode was used in conjunction with polysulfide to study the photocurrent conversion efficiency of the QD-nanowire structure.[12]

TABLE I. Calculated absolute values of the electron transition matrix elements for doped and undoped fragments.

Interface	Pb/ZTO	Mn/ZTO
Electronic coupling $\|V\|$	0.1928 eV	0.4947 eV

X-ray diffraction (XRD) was done on reference films using a Rigaku Smartlab diffractometer with a Cu-Kα source. X-ray reflectivity on the reference film sample helped find approximate thickness for the deposited films. Some nanowires were scraped and suspended in isopropyl alcohol which was then dropped onto a TEM grid. TEM was done with a FEI Tecnai G2 microscope.

Continuous wave-EPR measurement was performed with a Bruker EMX in X-band at room temperature. The reference film on Si was scraped off and suspended in dichloroethane for the measurement.

Absorption spectrum was recorded for the film deposited on quartz with a Cary50 UV-vis spectrophotometer. The incident photon to electron conversion efficiency spectrum (IPCE) was obtained with a home built system.

An Omicron low temperature scanning tunneling microscope (LT-STM) was used to perform STM and scanning tunneling spectroscopy (STS) measurements on PbS and Mn:PbS QDs prepared by PLD on As:Si(100) substrates. All scans were performed at liquid nitrogen temperature in an ultra-high vacuum (UHV) environment with a base pressure better than 1×10^{-11} mbar.

The quantum chemical calculations of PbS QDs with Mn impurities were performed within GAUSSIAN[23] and Amsterdam Density Functional (ADF)[24–26] computational packages. The initial geometry of a QD was adopted from the bulk structure by cutting out a sphere of a specified size. The doping is provided by replacing certain Pb atoms with Mn atoms. ZTO substrate was modeled by a slab of ZTO crystal. The interface region between ZTO and PbS (Mn:PbS) is then optimized within GAUSSIAN in the density functional theory formalism with a B3LYP exchange-correlation functional and 6–31+G* for Zn, Sn, O, S, and Mn atoms and SBKJC basis set for Pb atoms. The interface configuration is then used in ADF package with a B3LYP exchange-correlation functional and Triple-Zeta Polarized basis set on all the atoms to obtain the effective transfer integrals between ZTO and QD fragments.

This work was supported by the U.S. Department of Energy, Office of Basic Energy Sciences, Division of Materials Sciences and Engineering (DEFG02-10ER46728). G.R. and A.K.P. acknowledge the support from the School of Energy Resources of the University of Wyoming.

A.J.Y. acknowledges graduate fellowship support from the National Science Foundation and the University of Wyoming EE-Nanotechnology Program (NSF-DGE-0948027).

[1]J. Du, Z. Du, J.-S. Hu, Z. Pan, Q. Shen, J. Sun, D. Long, H. Dong, L. Sun, X. Zhong, and L.-J. Wan, "Zn–Cu–In–Se quantum dot solar cells with a certified power conversion efficiency of 11.6%," J. Am. Chem. Soc. **138**(12), 4201–4209 (2016).

[2]H. Zhou, Q. Chen, G. Li, S. Luo, T.-B. Song, H.-S. Duan, Z. H. Jingbi You, Y. Liu, and Y. Yang, "Interface engineering of highly efficient perovskite solar cells," Science **345**, 542 (2014).

[3]Q. Dai, E. M. Sabio, W. Wang, and J. Tang, "Pulsed laser deposition of Mn doped CdSe quantum dots for improved solar cell performance," Appl. Phys. Lett. **104**, 183901 (2014).

[4]P. K. Santra and P. V. Kamat, "Mn-doped quantum dot sensitized solar cells: A strategy to boost efficiency over 5%," J. Am. Chem. Soc. **134**, 2508 (2012).
[5]S. Horoz, Q. Dai, F. S. Maloney, B. Yakami, J. M. Pikal, X. Zhang, J. Wang, W. Wang, and J. Tang, "Absorption induced by Mn doping of ZnS for improved sensitized quantum-dot solar cells," Phys. Rev. Appl. **3**, 024011 (2015).
[6]J. B. Sambur, T. Novet, and B. A. Parkinson, "Multiple exciton collection in a sensitized photovoltaic system," Science **330**, 63 (2010).
[7]F. W. Wise, "Lead salt quantum dots: The limit of strong quantum confinement," Acc. Chem. Res. **33**, 773 (2000).
[8]G.-H. Kim, F. P. G. de Arquer, Y. J. Yoon, X. Lan, M. Liu, O. Voznyy, Z. Yang, F. Fan, A. H. Ip, P. Kanjanaboos, S. Hoogland, J. Y. Kim, and E. H. Sargent, "High-efficiency colloidal quantum dot photovoltaics via robust self-assembled monolayers," Nano Lett. **15**(11), 7691–7696 (2015).
[9]A. Pimachev and Y. Dahnovsky, "Optical and magnetic properties of PbS nanocrystals doped by manganese impurities," J. Phys. Chem. C **119**, 16941 (2015).
[10]R. Beaulac, P. I. Archer, X. Liu, S. Lee, G. M. Salley, M. Dobrowolska, J. K. Furdyna, and D. R. Gamelin, "Spin-polarizable excitonic luminescence in colloidal Mn^{2+}-doped CdSe quantum dots," Nano Lett. **8**, 1197 (2008).
[11]V. Proshchenko and Y. Dahnovsky, "Optical spectra of CdMnSe of nano-ferro- and antiferro-magnets," Phys. Chem. Chem. Phys. **17**, 26828 (2015).
[12]Q. Dai, J. Chen, L. Lu, J. Tang, and W. Wang, "Pulsed laser deposition of CdSe quantum dots on Zn_2SnO_4 nanowires and their photovoltaic applications," Nano Lett. **12**, 4187 (2012).
[13]Q. Dai, J. Chen, L. Lu, J. Tang, and W. Wang, "PbS quantum dots prepared by pulsed laser deposition for photovoltaic applications and ligand effects on device performance," Appl. Phys. Lett. **102**, 203904 (2013).
[14]R. S. Silva, P. C. Morais, F. Qu, A. M. Alcalde, N. O. Dantas, and H. S. L. Sullasi, "Synthesis process controlled magnetic properties of $Pb_{1-x}Mn_xS$ nanocrystals," Appl. Phys. Lett. **90**, 253114 (2007).
[15]F. Moro, L. Turyanska, J. Wilman, A. J. Fielding, M. W. Fay, J. Granwehr, and A. Patanè, "Electron spin coherence near room temperature in magnetic quantum dots," Sci. Rep. **5**, 10855 (2015).
[16]L. Turyanska, F. Moro, A. N. Knott, M. W. Fay, T. D. Bradshaw, and A. Patan, "Paramagnetic, near-infrared fluorescent Mn-doped PbS colloidal nanocrystals," Part. Part. Syst. Charact. **30**, 945 (2013).
[17]H. W. de Wijn and R. F. van Balderen, "Electron spin resonance of manganese in borate glasses," J. Chem. Phys. **46**, 1381 (1967).
[18]L. Turyanska, R. J. A. Hill, O. Makarovsky, F. Moro, A. N. Knott, O. J. Larkin, A. Patane, A. Meaney, P. C. M. Christianen, M. W. Fay, and R. J. Curry, "Tuneable paramagnetic susceptibility and exciton g-factor in Mn-doped PbS colloidal nanocrystals," Nanoscale **6**, 8919 (2014).
[19]A. Shabaev, Al. L. Efros, and A. J. Nozik, "Multiexciton generation by a single photon in nanocrystals," Nano Lett. **6**, 2856 (2006).
[20]H. Haug and A.-P. Jauho, "Quantum kinetics in transport and optics of semiconductors," in *Solid-State Sciences* (Springer, Berlin, Heidelberg, 2008), Vol. 123.
[21]J. Chen, L. Lu, and W. Wang, "Zn_2sno_4 nanowires as photoanode for dye-sensitized solar cells and the improvement on open circuit voltage," J. Phys. Chem. C **116**, 10841 (2012).
[22]A. Braga, S. Gimenez, I. Concina, A. Vomiero, and I. Mora-Sero, "Panchromatic sensitized solar cells based on metal sulfide quantum dots grown directly on nanostructured TiO_2 electrodes," J. Phys. Chem. Lett. **2**, 454 (2011).
[23]M. J. Frisch, G. W. Trucks, H. B. Schlegel, G. E. Scuseria, M. A. Robb, J. R. Cheeseman, G. Scalmani, V. Barone, B. Mennucci, G. A. Petersson, H. Nakatsuji, M. Caricato, X. Li, H. P. Hratchian, A. F. Izmaylov, J. Bloino, G. Zheng, J. L. Sonnenberg, M. Hada, M. Ehara, K. Toyota, R. Fukuda, J. Hasegawa, M. Ishida, T. Nakajima, Y. Honda, O. Kitao, H. Nakai, T. Vreven, J. A. Montgomery, Jr., J. E. Peralta, F. Ogliaro, M. Bearpark, J. J. Heyd, E. Brothers, K. N. Kudin, V. N. Staroverov, R. Kobayashi, J. Normand, K. Raghavachari, A. Rendell, J. C. Burant, S. S. Iyengar, J. Tomasi, M. Cossi, N. Rega, J. M. Millam, M. Klene, J. E. Knox, J. B. Cross, V. Bakken, C. Adamo, J. Jaramillo, R. Gomperts, R. E. Stratmann, O. Yazyev, A. J. Austin, R. Cammi, C. Pomelli, J. W. Ochterski, R. L. Martin, K. Morokuma, V. G. Zakrzewski, G. A. Voth, P. Salvador, J. J. Dannenberg, S. Dapprich, A. D. Daniels, Farkas, J. B. Foresman, J. V. Ortiz, J. Cioslowski, and D. J. Fox, *Gaussian 09 Revision E.01* (Gaussian Inc., Wallingford, CT, 2009).
[24]ADF2014, *SCM, Theoretical Chemistry* (Vrije Universiteit, Amsterdam, The Netherlands, 2014).
[25]G. te Velde, F. M. Bickelhaupt, E. J. Baerends, C. Fonseca Guerra, S. J. A. van Gisbergen, J. G. Snijders, and T. Ziegler, "Chemistry with ADF," J. Comput. Chem. **22**, 931 (2001).
[26]C. Fonseca Guerra, G. J. Snijders, G. te Velde, and J. E. Baerends, "Towards an order-n DFT method," Theor. Chem. Acc. **99**, 391 (1998).